

Explaining Deviations from the Scaling Relationship of the Large Frequency Separation

JOEL ONG J. M. (王加冕)¹ AND SARBANI BASU¹¹*Department of Astronomy, Yale University, 52 Hillhouse Ave., New Haven, CT 06511, USA*

(Dated: November 15, 2018; Received September 11, 2018; Accepted November 15, 2018)

Submitted to ApJ

ABSTRACT

Asteroseismic large frequency separations possess great diagnostic value. However, their expressions as scaling relations are predicated on homology arguments which may not hold in general, resulting in mass- and temperature-dependent deviations. The first-order asymptotic expressions, which should in principle account for this structural evolution, also deviate more from fitted frequency-separation estimates than do the simple scaling relations, and exhibit qualitatively different behavior. We present a modified asymptotic estimator, and show that these discrepancies can be accounted for by the evolution of the acoustic turning points of the asteroseismic mode cavity, which is typically neglected in first-order asymptotic analysis. This permits us to use a single expression to accurately estimate the large frequency separations of main-sequence, ascending red giant branch, and red clump stellar models, except at transition points between two asymptotic regimes during the subgiant phase of evolution, where the WKB approach fails. The existence of such transition points provides theoretical justification for separately calibrated scaling relations for stars in different evolutionary stages.

Keywords: methods: analytical, methods: numerical, stars: oscillations

1. INTRODUCTION

Solar-like oscillations — oscillations of the star excited stochastically in convective envelopes — result in photometric and velocity variations which have frequency-domain power spectra that exhibit a comb-like structure. Such a comb is composed of peaks at the resonant frequencies of global asteroseismic p-modes, which are (to a good approximation) evenly spaced in the frequency domain with a characteristic spacing $\Delta\nu$, which is called the large frequency separation. Phenomenologically, there exist minor variations in the mode frequency spacing (owing to e.g. acoustic glitches), and in practice an average value of $\Delta\nu$ is found by least-squares fitting of mode frequencies against their associated radial quantum numbers, with appropriate weights to account for variations of noise and mode amplitudes.

The asymptotic expression for these p-mode frequencies,

$$2\nu_{nl}T_0 = n + \frac{l}{2} + \alpha, \quad (1)$$

where $T_0 = 2 \int_0^R \frac{dr}{c_s}$ is the sound-travel time, yields an expression for the large frequency separation of radial modes as

$$\Delta\nu_{n,0} = \nu_{n+1,0} - \nu_{n,0} \sim \frac{1}{2T_0}. \quad (2)$$

Under assumption of hydrostatic equilibrium, the sound-travel time and gravitational dynamical time $T_{\text{ff}} \sim 1/\sqrt{G\bar{\rho}}$ should be of roughly the same order of magnitude, giving rise to the scaling relation (Ulrich 1986; Christensen-Dalsgaard 1988)

$$\frac{\Delta\nu}{\Delta\nu_{\odot}} \sim \sqrt{\frac{\bar{\rho}}{\bar{\rho}_{\odot}}}, \quad (3)$$

with $\bar{\rho}$ as the mean density of the star, for stars that are essentially homologous to the Sun. This solar-calibrated scaling relation has been historically established to hold relatively well even for stellar models that exhibit considerable structural differences from the Sun. For this

reason, the large separation has proven to be a valuable diagnostic of global properties of stars exhibiting such solar-like oscillations (Chaplin et al. 2014; Pinsonneault et al. 2014; Serenelli et al. 2017).

Owing to this first-order dependence on the mean density, observational measurements of $\Delta\nu$ have been widely applied to determine asteroseismic estimates of stellar masses and radii, either by direct inversion of this scaling relation (e.g. Chaplin et al. 2010), or through a so-called grid-based approach, where an optimal solution is determined from the large separations of a grid of models (e.g. Basu et al. 2011; Chaplin et al. 2014; Pinsonneault et al. 2014). For the latter case, it is generally desirable to be able to accurately estimate $\Delta\nu$ from a stellar model without solving for individual mode frequencies, which is quite computationally expensive. The scaling relation is typically used for this purpose.

However, there remain discrepancies (of order a few percent) between the scaling relation predictions compared to fitted values of $\Delta\nu$ as computed from detailed frequencies returned from stellar models (i.e. even in the absence of observational errors and unconstrained physics), which prevent its use in such a capacity in the regime of high-precision asteroseismology. White et al. (2011) find that these scaling deviations appear to exhibit some dependence on the effective temperature (and by proxy on stellar evolution — see Fig. 1), with an apparent second-parameter dependence on stellar metallicity.

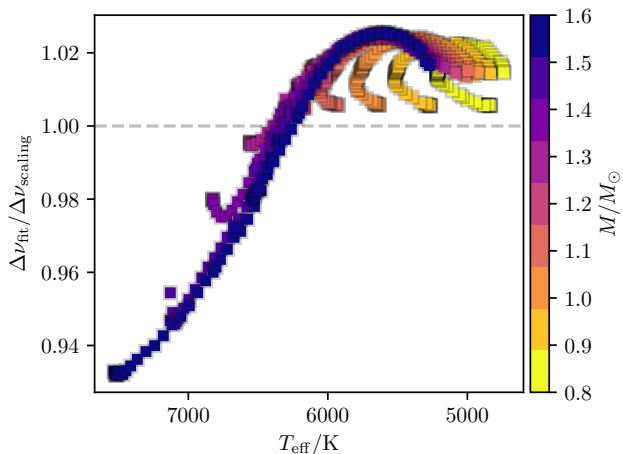


Figure 1. Scaling deviations: ratio of fitted $\Delta\nu$ versus scaling relation estimator for solar-metallicity main-sequence/subgiant MESA stellar models with solar-calibrated parameters over a range of stellar masses.

Extant approaches to dealing with these deviations vary, but are uniformly empirical in nature. For instance, White et al. (2011) fit a parabola to the empirical morphology of the scaling deviation curve, while Guggenberger et al. (2016) propose the use of a damped-sinusoid

function (with additional modifications from symbolic regression presented in Guggenberger et al. 2017), and Kallinger et al. (2018) propose modifying the first-order expression Eq. (1) to include additional free parameters, accounting for acoustic glitches and second-order curvature effects, resulting in additional terms in the scaling relation that have to be calibrated empirically. Sharma et al. (2016) instead seek recourse to explicitly calibrating the scaling deviations against a reference grid of stellar models spanning the desired parameter space. While undoubtedly practical, such approaches lack theoretical insight. Moreover, attempts at empirical fits (without recourse to a model grid) have neglected scaling deviations on the main sequence, despite these stars being in principle the most similar to the Sun (and hence ostensibly the easiest to model).

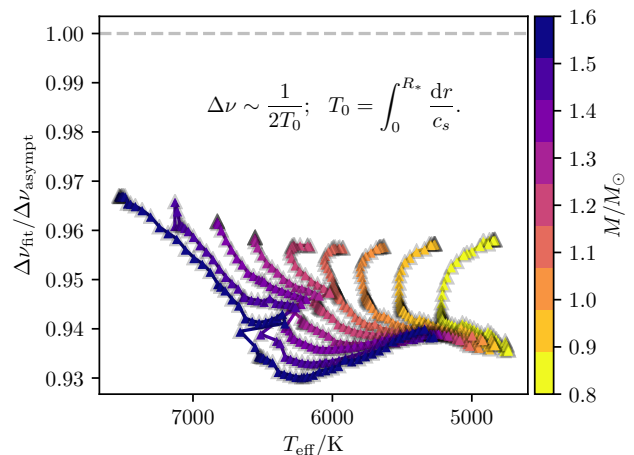


Figure 2. Ratio of fitted $\Delta\nu$ versus the usual asymptotic estimator (i.e. sound-travel time) for the same set of stellar models as Fig. 1.

While the sound-travel time may also be used to estimate $\Delta\nu$ without requiring individual mode frequencies, there exists some contention as to the correct choice of the upper limit R used to compute it. Strictly speaking, the limit of integration should be the outer boundary of the eigenvalue problem with respect to which the eigenfunctions are computed. However, this boundary is difficult to define. While the photospheric radius is used by default in most evolutionary codes, it returns sound-travel times that are typically lower (and therefore frequency separations higher) than would be consistent with both observational values and values fitted against detailed model frequencies (as in Fig. 2). Hekker et al. (2013) note that this can be remedied by simply extending the domain of integration outwards, but the question of ambiguity as to the correct outer boundary remains.

A critical underlying assumption made in all of these analyses is that the phenomenological and asymptotic values of $\Delta\nu$ should be similar, which is only true if the

phase function α in Eq. (1) does not exhibit significant secular variation between modes. This would be the case with e.g. the contribution to α from an acoustic glitch, where the rapid but oscillatory variations with frequency are cancelled out when a global value of $\Delta\nu$ is fitted for. However, in this formulation, the value of α as a function of frequency depends on the structure of the entire stellar model, and this assumption may not necessarily hold good. On the other hand, should such secular phase variations exist, their dependence on stellar parameters like the mass and radius is not *a priori* obvious.

We derive instead an asymptotic estimator for the large frequency separation which captures most of the variation in these phase functions (and so scaling deviations) with a single expression, and thereby returns estimates of $\Delta\nu$ that are considerably closer to the fitted value than the traditional asymptotic estimator, without any ambiguity as to the outer turning point of the relevant integral. We demonstrate numerically that the validity of this expression is independent of stellar mass, evolutionary stage (with one major exception), and atmospheric model.

2. THE WKB APPROXIMATION

2.1. Review of existing work

In the first-order asymptotic theory of p-modes, the large frequency separation $\Delta\nu$ emerges from the phase integral quantization condition

$$\int_{r_1}^{r_2} k_r(r, \omega) dr = \pi(n + \kappa) \quad (4)$$

for integer n , where k_r is the WKB wavenumber, r_1 and r_2 are the turning points of the integral (usually where k_r vanishes), and κ is a function of frequency. Here, κ depends only on the functional behavior of k_r^2 at the turning points. In particular it can be shown that $\kappa = -\frac{1}{2}$ is constant if $k_r^2 \propto r - r_t$ at both turning points (Gough 2007; Aerts et al. 2010). To a first approximation, this expression yields the Duvall law,

$$\int_{r_t}^R \frac{dr}{c_s} \sqrt{1 - \frac{S_l^2}{\omega^2}} = \pi \left(\frac{n + \kappa}{\omega} \right), \quad (5)$$

where c_s is the sound speed, $S_l^2 = \frac{l(l+1)}{c_s^2 r^2}$ is the Lamb frequency, and $\omega = 2\pi\nu$ is the angular frequency. Again the inner turning point of this integral is defined by where the integrand vanishes (or $r = 0$ for radial modes), and the outer turning point R is the same as that used to evaluate the sound-travel time.

Naturally, higher-order approximations are possible. For instance, Tassoul (1994) derives Eq. (1) from a second-order expansion of the asteroseismic equations of motion, using linear combinations of spherical Bessel functions and their derivatives as ansatz for the eigenfunctions, with a similar phase integral quantization condition

emerging for the arguments of these functions. This was in turn taken to fourth order by Roxburgh & Vorontsov (1994) with a similar approach.

On the other hand, the accuracy of the WKB expression can also be improved with more detailed asymptotic analysis (i.e. not setting terms to zero prematurely before performing the WKB analysis). For instance, a more accurate description is afforded by Deubner & Gough (1984):

$$\int_{r_1}^{r_2} \frac{dr}{c_s} \sqrt{1 - \frac{\omega_{ac}^2}{\omega^2} - \frac{S_l^2}{\omega^2} \left(1 - \frac{N^2}{\omega^2} \right)} = \pi \left(\frac{n + \kappa'}{\omega} \right), \quad (6)$$

which emerges from just such a more detailed analysis (with still more detail provided in Gough 1993). This integrand in this expression reduces asymptotically to that in Eq. (5) far into the interior of the convective envelope of solar-like main-sequence stars, where $\omega_{ac} \ll \omega$ for most p-modes of interest. Here N^2 is the Brunt-Väisälä or buoyancy frequency, and κ' is another function of frequency (different in general from κ in Eq. (5)). However, κ' also only depends on the behavior of the integrand in Eq. (6) at the turning points.

The formulation of Eq. (6) differs from the standard form of the Duvall law both in terms of its explicit dependence on an acoustic cutoff frequency

$$\omega_{ac}^2 = \frac{c_s^2}{4H^2} \left(1 - 2 \frac{dH}{dr} \right), \quad (7)$$

involving $H = - \left(\frac{d \ln \rho}{dr} \right)^{-1}$ (the density scale height) in the integrand, and in terms of the locations of the turning points (as the integrands vanish at different places). In particular, the outer turning point is essentially determined by the acoustic cutoff frequency, rather than being defined by the boundary conditions of the eigenvalue problem. The precise form of the acoustic cutoff frequency, and other quantities involved in the oscillation equations, will depend on the choice of dynamical variable used to perform the WKB analysis. Nonetheless, the resulting eigenvalue equation can typically be put into the form of Eq. (6), although different expressions for ω_{ac} , S_l^2 and N^2 may have to be used in place of those described here. An illustrative example can be found in Gough (1993).

With respect to the above formalism, Christensen-Dalsgaard & Perez Hernandez (1992) instead define a phase function α so that

$$\int_{r_t}^R \frac{dr}{c_s} \sqrt{1 - \frac{S_l^2}{\omega^2}} = \pi \left(\frac{n + \alpha}{\omega} \right), \quad (8)$$

where

$$\alpha(\omega) = \frac{\omega}{\pi} (T_1 - T_2) + \kappa', \quad (9)$$

with

$$\begin{aligned} T_1 &= \int_{r_t}^R \frac{dr}{c_s} \sqrt{1 - \frac{S_l^2}{\omega^2}}, \\ T_2 &= \int_{r_1}^{r_2} \frac{dr}{c_s} \sqrt{1 - \frac{\omega_{ac}^2}{\omega^2} - \frac{S_l^2}{\omega^2} \left(1 - \frac{N^2}{\omega^2}\right)} \end{aligned} \quad (10)$$

being integrals with dimensions of time appearing on the LHS of Eqs. (5) and (6). This permits the use of Eq. (1) with α in place of κ . Whereas the phase functions κ and κ' defined previously depend only locally on the asymptotic properties of the WKB integrands in the neighborhoods of their classical turning points, α as defined in this manner depends also on global properties of the entire acoustic mode cavity.

2.2. A new expression

We take the first-order expression Eq. (6) at face value, and assume that the quantities N^2 and S_l^2 have no parametric dependence on the frequency, and further that all quantities on the RHS are continuous functions of the frequency ν . We proceed to expand finite differences as Taylor series. In particular, we consider finite differences of the terms in Eq. (6), multiplied throughout by $\omega/\pi = 2\nu$ and evaluated at frequencies of adjacent n for the same l :

$$\begin{aligned} &2\nu_{n+1,l}T_2(\nu_{n+1,l}) - 2\nu_{n-1,l}T_2(\nu_{n-1,l}) \\ &\quad \sim 2 + \kappa'(\nu_{n+1,l}) - \kappa'(\nu_{n-1,l}) \quad (11) \\ \implies &4 \frac{d\nu T_2}{d\nu} \Delta\nu \sim 2 + 2 \frac{d\kappa'}{d\nu} \Delta\nu, \end{aligned}$$

with the quantities on the last line being evaluated at the frequency $\nu = \frac{1}{2}(\nu_{n+1,l} + \nu_{n-1,l})$ so that the error term is $\mathcal{O}(\Delta\nu^3)$, and where T_2 is the LHS of Eq. (6). This yields the expression

$$\Delta\nu \sim \left(2 \frac{d\nu T_2}{d\nu} - \frac{d\kappa'}{d\nu}\right)^{-1}. \quad (12)$$

For the first term, we observe that

$$\begin{aligned} &\frac{d}{d\nu} \left(\nu \int_{r_1}^{r_2} \sqrt{f(r, \nu)} \frac{dr}{c_s} \right) = \frac{d}{d\omega} \left(\omega \int_{r_1}^{r_2} \sqrt{f(r, \omega)} \frac{dr}{c_s} \right) \\ &= \int_{r_1}^{r_2} \frac{f(r, \omega) + \frac{1}{2}\omega \frac{\partial}{\partial \omega} f(r, \omega)}{\sqrt{f(r, \omega)}} \frac{dr}{c_s} \\ &+ \omega \left(\frac{\sqrt{f(r_2, \omega)} \frac{dr_2}{d\omega}}{c_s} - \frac{\sqrt{f(r_1, \omega)} \frac{dr_1}{d\omega}}{c_s} \right). \end{aligned} \quad (13)$$

Since the turning points of the integral are either fixed (for $r_1 = 0$) or defined to be where the relevant integrand vanishes, the boundary contributions to the above derivative also vanish, leaving us with

$$2 \int_{r_1}^{r_2} \frac{dr}{c_s} \frac{1 - \frac{S_l^2 N^2}{\omega^4}}{\sqrt{1 - \frac{\omega_{ac}^2}{\omega^2} - \frac{S_l^2}{\omega^2} \left(1 - \frac{N^2}{\omega^2}\right)}} - \frac{d\kappa'}{d\nu} \quad (14)$$

inside the parentheses in Eq. (12). For radial modes in particular, we can neglect S_l^2 , leaving us with

$$\Delta\nu \sim \left(2 \int_{r_1}^{r_2} \frac{dr}{c_s} \frac{1}{\sqrt{1 - \frac{\omega_{ac}^2}{\omega^2}}} - \frac{d\kappa'}{d\nu}\right)^{-1}. \quad (15)$$

As noted previously, $\kappa' = -\frac{1}{2}$ in the ideal WKB scenario of the mode cavity exhibiting asymptotically linear behavior near the classical turning points. On the other hand, if the radicand tends to a constant value near the inner turning point (as would be the case for Sun-like stars, where $\omega_{ac} \ll \omega$ far into the interior), then the behavior of the eigenfunctions near the inner turning point are described by the spherical Bessel function j_0 , and $\kappa' = -\frac{1}{4}$ (Gough 1993). In either case, assuming that it changes very slowly with respect to frequency, its derivative is much smaller than the integral expression. We thus propose the use of a modified integral estimator for the large frequency separation:

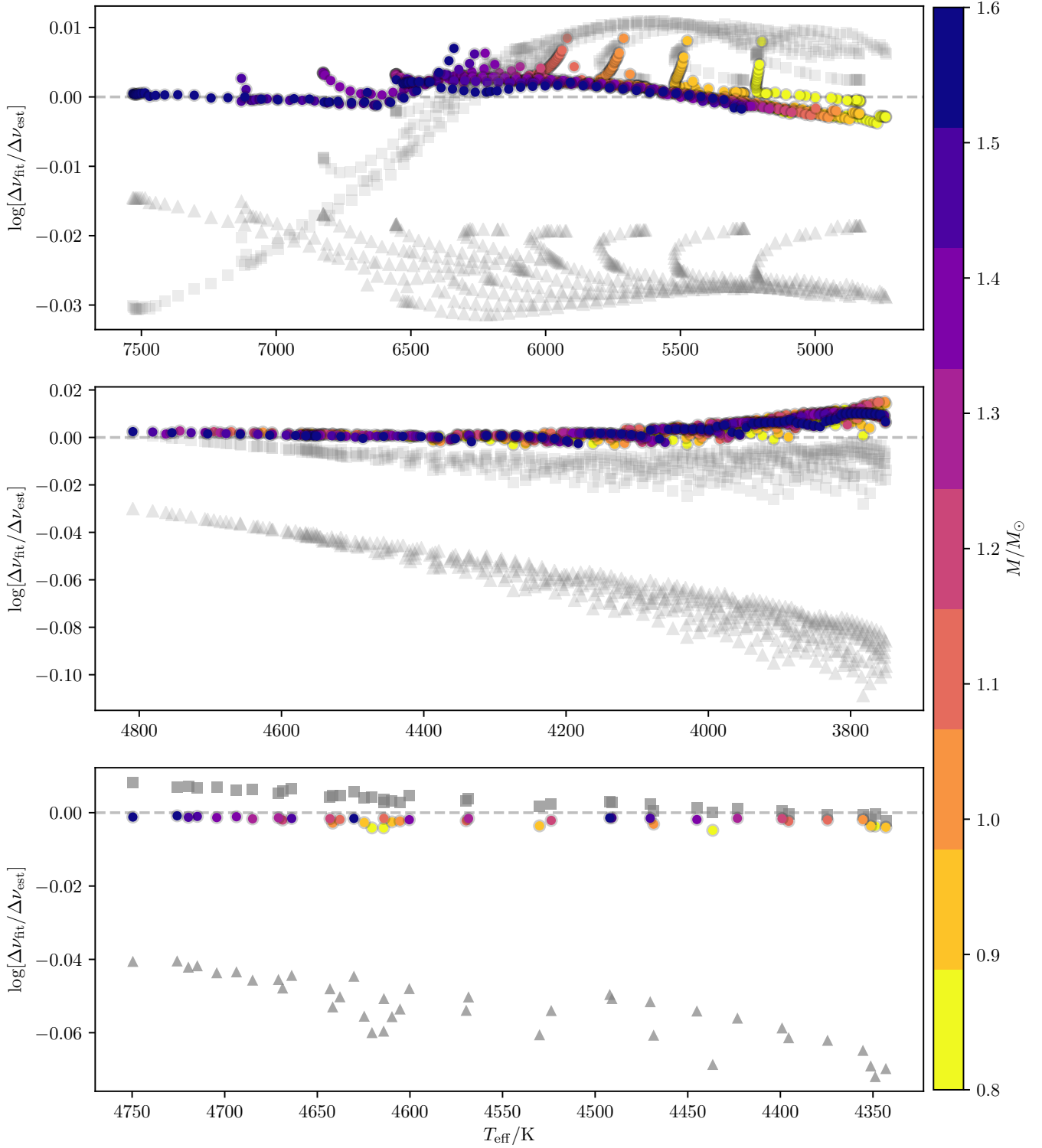
$$\Delta\nu \sim \left(2 \int_{r_1}^{r_2} \frac{dr}{c_s} \frac{1}{\sqrt{1 - \frac{\omega_{ac}^2}{\omega^2}}}\right)^{-1}. \quad (16)$$

This expression contains an explicit dependence on the frequency. Observationally, however, we are limited to the study of only modes with frequencies near ν_{\max} , the frequency of maximum acoustic power. Moving forward, we will evaluate this quantity at ν_{\max} .

We note that the denominator of the integrand in Eq. (16) vanishes at the outer boundary of the domain of integration, so the integrand becomes singular. Depending on the acoustic cutoff frequency of the stellar model, this may also be the case at the inner boundary. In the ideal WKB regime, this results in the presence of integrable singularities at the endpoints. We would therefore expect that the evolution of these turning points plays a significant role in how the value of this estimator changes over the course of stellar evolution. Our expression does not contain a prescription for the actual turning points of the asymptotic integral, only that they depend on the formulation of the acoustic cutoff frequency that accompanies the degree of approximation being used.

Moreover, within the domain of integration, we note that the integrand is strictly larger than the $1/c_s$ that appears as the integrand of the sound-travel time. Since the integrand is also strictly positive, we conclude that the integral is strictly larger than the sound-travel time. Given that the sound-travel time generally overestimates $\Delta\nu$ (i.e. yields too small a value of the integral, as in Fig. 2), this is suggestive as at least a zeroth-order mark of improvement.

3. BENCHMARKING AGAINST MODELS



Our modified estimator for $\Delta\nu$, Eq. (16), was derived under assumptions that may not be strictly valid in all cases. To test how well it actually reproduces the large separation of a model, we compare it against $\Delta\nu$ as calculated using the frequencies of a model.

To do this, we compute both Eq. (16) as well as an estimate of $\Delta\nu$ from a linear fit to individual mode frequencies, for a variety of stellar models constructed with the stellar evolution code MESA, version 10398 (Paxton et al. 2015). We ran evolutionary tracks for stellar masses from 0.8 to 1.6 solar masses in increments of $0.1M_\odot$, using initial helium abundances Y_0 and mixing-length parameters α_{MLT} obtained by constructing solar-calibrated models at solar metallicity (using values from Grevesse & Sauval 1998), but with no additional constraints. Frequencies were computed with version 5.1 of the GYRE oscillation code (Townsend & Teitler 2013). The evolution included heavy element diffusion and gravitational settling as well as convective overshoot. We compute frequencies for all radial modes up until the maximum acoustic cutoff frequency (i.e. all trapped p-modes)

As noted above, our proposed asymptotic estimator has an explicit frequency dependence, and we evaluate it at the frequency of maximum acoustic power, ν_{max} . While the theoretical underpinnings of ν_{max} are not well-understood, it carries diagnostic information on the excitation and damping of stellar modes, and hence must depend on the physical conditions in the near-surface layers where the modes are excited. Close to the surface (and outer acoustic turning point), the behavior of the waves is strongly influenced by the acoustic cut-off frequency. Brown et al. (1991) argue that $\nu_{\text{max}} \propto \nu_{\text{ac}}$, since both frequencies are determined by conditions in the near-surface layers; Kjeldsen & Bedding (1995) use this to derive a scaling relation between ν_{max} and near-surface properties. Belkacem et al. (2011) show that while ν_{max} does indeed depend on ν_{ac} , there are also additional dependences on other quantities, such as the turbulent Mach number and the mixing-length parameter. However, to simplify matters, in this work we evaluate Eq. (16) at the value of ν_{max} given by the scaling relation of Kjeldsen & Bedding (1995).

The expression Eq. (7) for the acoustic cutoff frequency exhibits rapid variations, both owing to limitations in the MESA models and possibly density discontinuities, which may affect the accuracy of the WKB approximation (in that k_r may not vary slowly). In particular, large rapid variations near the turning points will strongly influence the computed value of the integrable singularities there. To avoid this, we use an isothermal homogeneous plane-parallel ideal-gas approximation, as detailed in Aerts et al. (2010). Practically, this means that we use only the leading order term in Eq. (7) when computing the acoustic cutoff frequency. In turn, the value of

the integral Eq. (16) was evaluated using an adaptive Gauss-Kronrod quadrature scheme.

3.1. Results

To compare the results obtained from the integral and from frequencies, we compute the logarithms of the ratios between the value of $\Delta\nu_{\text{fit}}$ (obtained by a least-squares fit of $\nu_{n,l=0}$ against n), versus the values of our integral estimator in Eq. (16), which we plot as circles in subsequent figures. We also do this with the log ratios of $\Delta\nu_{\text{fit}}$ versus the values of the sound-travel time estimator $1/2T_0$ (which we show as upright triangles), as well as versus the values predicted by the scaling relation (squares). As a more quantitative (but still heuristic) comparison, we compute the root-mean-square (RMS) deviation of these log-ratios from zero. An RMS deviation of zero means that the estimator exactly coincides with $\Delta\nu_{\text{fit}}$ for all models.

The top panel of Fig. 3 shows the values of the log ratios described above for stellar models along the main sequence and on the subgiant branch. It is visually evident that the agreement between the estimator in Eq. (16) and the fitted values of $\Delta\nu$ is considerably better than both the scaling relation and the sound-travel time. We find that the scaling relation results in a RMS log-deviation of about 0.010 dex, compared to 0.025 dex for the sound-travel time and 0.002 dex for our integral estimator.

Whereas the relative deviations from the scaling relation appear to exhibit curlicues for main-sequence stars of different masses (as in Fig. 1), we note that the most obvious deviations between our asymptotic estimator and the fitted value of $\Delta\nu$ occur as a sharp spike near main-sequence turnoff during the onset of shell burning (at core hydrogen exhaustion/subgiant hook for more massive stars). We examine this more closely with Fig. 4.

We show in the top panel of Fig. 4 the acoustic cut-off frequency, in units of ν_{max} , of main-sequence, MS turnoff, and subgiant stellar models with $M = 1.0M_\odot$. Following our above discussion of various values of κ in the WKB regime, we see that for the main-sequence star (blue solid curve), the inner turning point is at $r = 0$, where $\nu_{\text{ac}}/\nu_{\text{max}} \ll 1$, and the WKB wavefunction goes as $j_0(\omega t)$, where $t \sim \int_0^r \sqrt{1 - (\omega_{\text{ac}}/\omega)^2} \frac{dr}{c_s}$, with the same integrand as in Eq. (6). On the other hand, for the subgiant star (green dashed curve), the WKB wavefunction goes as $\text{Ai}(-|\omega t|^{3/2})$ near a first-order classical turning point at $r = r_1$, where $\nu_{\text{ac}}(r_1) \sim \nu_{\text{max}}$ and $t \sim \int_{r_1}^r \sqrt{1 - (\omega_{\text{ac}}/\omega)^2} \frac{dr}{c_s}$, and Ai is the Airy function.

These represent two distinct asymptotic regimes in which the assumptions underlying the WKB approximation hold well. However, this is not necessarily true during the transition between these two regimes. In particular, for

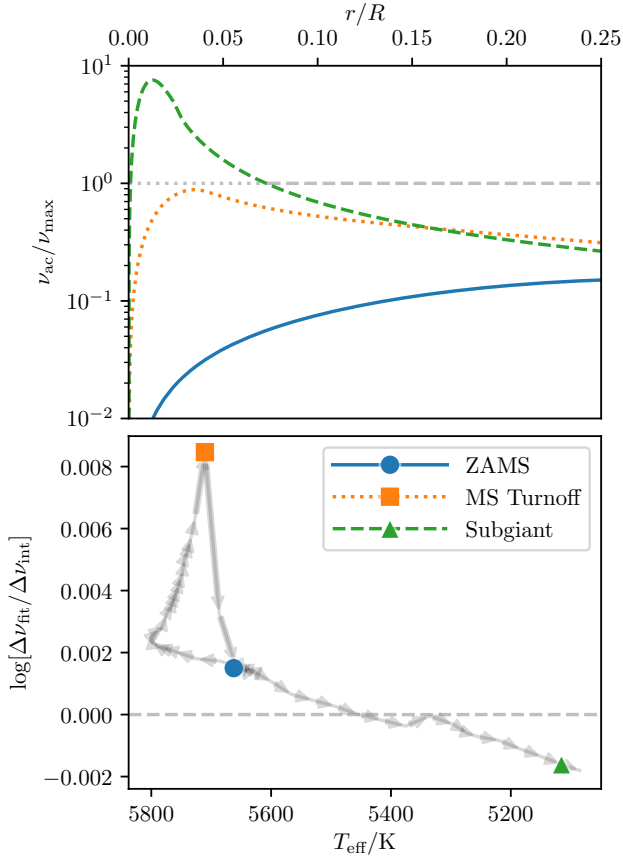


Figure 4. Top: Plots of the acoustic cutoff frequency in units of ν_{max} for stellar models at various evolutionary stages along the $1M_{\odot}$ track, showing the two extreme asymptotic regimes of the inner turning points for main-sequence and evolved stars, and illustrating the failure of the WKB approximation during the transition between them at main-sequence turnoff. **Bottom:** Log-ratio of frequency separations (as in top panel of Fig. 3) for $1M_{\odot}$ track, with direction of evolution indicated with arrows. Stellar models corresponding to curves shown in the top panel are marked out with points of the same color, on lines with corresponding linestyles, in the legend of the bottom panel.

some stellar models near main-sequence turnoff (yellow dotted curve), we have a maximum of the acoustic cutoff frequency with a value very close to ν_{max} . This violates one of the underlying assumptions of the WKB approximation (viz. that k_r varies slowly except near classical turning points, which requires in this case that $\nu \gg \nu_{ac}$), and neither of the above asymptotic descriptions is a good approximation for the actual mode eigenfunctions.

We have earlier noted that the radicand in Eq. (16) vanishes where $\nu_{ac} = \nu_{max}$. For first-order turning points, this results in integrable singularities at the endpoints of integration. However, when there is a maximum point where $\nu_{ac}/\nu_{max} \sim 1$ (as would be the case with a second-

order turning point), the integrand either changes very rapidly (becoming very large) in a region smaller than the wavelength of the eigenfunction ($\max \nu_{ac}/\nu_{max} \lesssim 1$), or a nonintegrable singularity is introduced into the domain of integration ($\max \nu_{ac}/\nu_{max} = 1$), and the convergence of the numerical integration is poor. In these cases, a numerical computation of Eq. (16) will be very different from the fitted value of $\Delta\nu$: the yellow dotted curve of Fig. 4 corresponds to the maximum deviation between Eq. (16) and the fitted value of $\Delta\nu$ along our $1M_{\odot}$ track (as in the yellow point of the bottom panel). In principle, the phase function κ , as we have defined it, also becomes discontinuous in the neighbourhood of $\nu = \max \nu_{ac} \sim \nu_{max}$, and its derivative also becomes singular. A proper accounting should permit these two singularities to cancel each other out. However, this is difficult to handle numerically.

It is possible that these difficulties can be resolved by a more refined analysis. For instance, strictly speaking, the asymptotic behavior of the WKB wavefunction near such a second-order stationary point should be given by the parabolic cylinder function (Gough 2007). However, such an analysis is fairly involved, and may not as readily yield a simple (and easily computed) expression like Eq. (16). Alternatively, one might imagine choosing a set of dynamical variables such that the expression for the cutoff frequency is always singular near the center of the model (Gough 1993), so that this transition point does not emerge. Again, doing so would require a more detailed analysis than we have performed, which we leave beyond the scope of this paper.

3.1.1. RGB and Red Clump stars

In the lower two panels of Fig. 3, we show the log-ratios of frequency-separation estimators for ascending RGB (middle panel) and descending RGB and red clump stars (lower panel). Once again, our expression in Eq. (16) deviates much less from the fitted $\Delta\nu$ than do both the scaling relation prediction and the sound-travel time. However, we note the emergence of terrace-like features in these deviation plots, which ultimately originate from the method by which we compute a fitted value for $\Delta\nu$. In particular, since we have included all modes with frequencies lower than the maximum acoustic cutoff frequency in the least-squares fit, and since the acoustic cutoff frequency changes relative to $\Delta\nu$ over the course of stellar evolution, the number of modes used in the fit changes also changes discontinuously over the course of the track, as illustrated in Fig. 5. These terraces are therefore a property of our benchmarking methodology, rather than being a feature of our asymptotic estimator.

In addition, we observe that while the scaling relation overpredicts the large frequency separation for ascending RGB stars, it instead slightly underpredicts it for red clump stars. Since the use of the scaling relation is

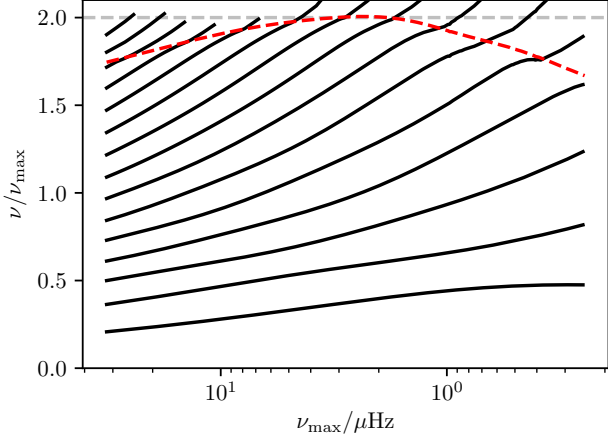


Figure 5. Frequencies of radial modes (in units of ν_{\max}) for stellar models on the ascending red giant branch from the $1M_{\odot}$ evolutionary track, with modes of the same n at different models being joined with solid lines. The maximum acoustic cutoff frequency in the atmosphere is shown with the red dashed line; only modes below this dashed line have a confined mode cavity, and so only these are included in the fit for $\Delta\nu$. As the age of the star increases (with decreasing effective temperature), this cutoff decreases relative to $\Delta\nu$, and so the number of modes available to be included in the fit decreases discontinuously.

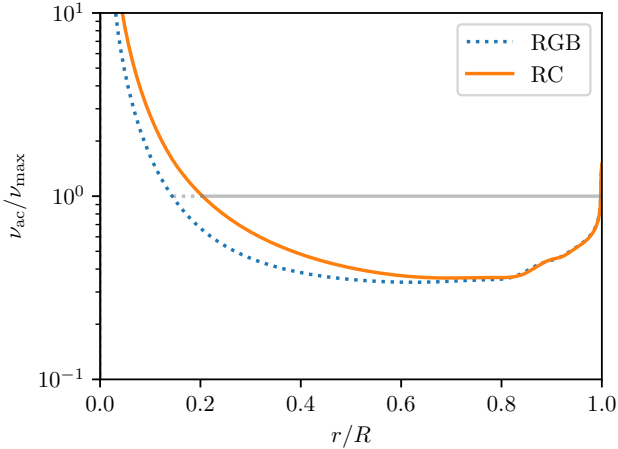


Figure 6. Acoustic cutoff frequency (in units of ν_{\max}) for two $1M_{\odot}$ stellar models on the ascending RGB (dotted line) and red clump (solid line) with the same $\log g$ (and therefore the same radii). While their acoustic structure is very similar near the envelope, the inner turning points of the modified radial p -mode cavity are different, as are the estimated values of $\Delta\nu$.

(implicitly) a homology argument (Belkacem et al. 2013), this indicates that the acoustic structure of red clump stars differs significantly from red giant stars. On this basis, Miglio et al. (2012) propose the use of different correction factors for the scaling relation for first-ascent red giant and red clump stars, precisely to account for these structural differences.

In terms of our formulation, we show in Fig. 6 the radial dependence of the acoustic cutoff frequency for two stellar models — one red giant and one red clump — with identical masses and radii. While their acoustic structure is very similar in the outer parts of the star, we see that their modified radial mode cavities have different inner turning points. Accordingly, our integral estimator correctly returns different estimates for $\Delta\nu$ for these different types of stars.

3.1.2. Dependence on Model Atmospheres

The models previously discussed were constructed with Eddington-grey atmospheres. To examine the dependence of our integral estimator on atmospheric conditions, we also constructed models using Krishna-Swamy model atmospheres, with Y_0 and α_{MLT} calibrated separately. Once again, we show the log ratios between our estimator and the fitted $\Delta\nu$ in the top panel of Fig. 7. Surprisingly, there does not appear to be any significant difference in the structure of the residuals. We interpret this to indicate that the remaining deviations that persist in either case stem from either an insufficiently high order of approximation, or from issues with our formulation that become significant only in the interior of the star, rather than the atmosphere.

One possible such inadequacy in our formulation could be our numerical treatment of the acoustic cutoff frequency — for example, Gough (1993) constructs a different expression for the acoustic cutoff frequency that takes the sphericity of the star into account, which only becomes significant deep in the stellar interior. This is also, therefore, where we expect the expression that we have used to be the most inaccurate. Since a large contribution to the value of our integral expression comes from singularities (integrable or otherwise) at the turning points, it is possible that the remaining error could potentially be considerably reduced, or eliminated entirely, by using an expression that is more accurate in the interior.

3.1.3. Dependence on metallicity

To investigate dependences on composition, we also construct stellar models with metallicities $[\text{Fe}/\text{H}] = \pm 0.5$, showing the log-ratios between the fitted frequency separation and our estimator in the bottom two panels of Fig. 7. We show only models possessing outer convection zones. We note that, aside from some translation along

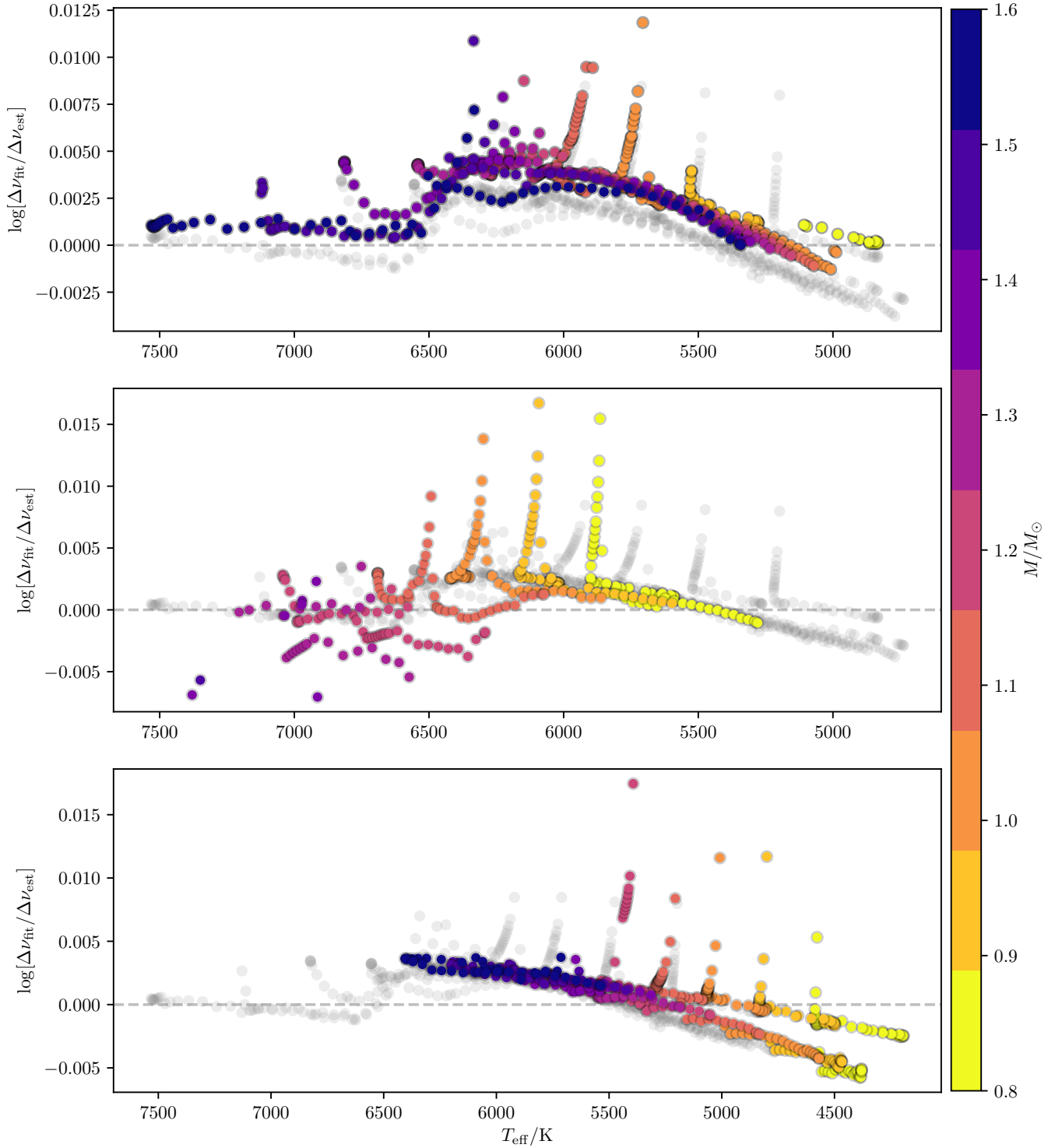


Figure 7. Log ratio of fitted $\Delta\nu$ versus our integral estimator for main-sequence/subgiant models with different physics and/or fundamental parameters. The grey points in the background correspond to the colored points in Fig. 3, at solar metallicity and with Eddington-grey atmospheres. **Top:** Models with Krishna-Swamy atmospheres instead of Eddington-grey atmospheres; **Middle:** Low-metallicity models (i.e. $[\text{Fe}/\text{H}] = -0.5$), excluding models with no outer convection zone (where we would not expect global oscillations to be excited at all); **Bottom:** High-metallicity models (i.e. $[\text{Fe}/\text{H}] = +0.5$).

the apparent residual curve, the qualitative features of these residuals are once again essentially unchanged.

3.1.4. $\Delta\nu$ from nonradial modes

Finally, if we relax our previous restriction to radial modes, we arrive at a similar integral expression

$$\Delta\nu_l \sim \left(2 \int_{r_1}^{r_2} \frac{dr}{c_s} \frac{1 - \frac{S_l^2 N^2}{\omega^4}}{\sqrt{1 - \frac{\omega_{ac}^2}{\omega^2} - \frac{S_l^2}{\omega^2} \left(1 - \frac{N^2}{\omega^2}\right)}} \right)^{-1} \quad (17)$$

for the large separation of modes with $l \neq 0$. To test this expression, we evaluate

$$\Delta\nu_l \sim \nu_{n+1,l} - \nu_{n,l} \quad (18)$$

by least-squares fitting of $\nu_{n,l}$ against n for $l = 1$ and 2 on the same set of stellar models as used in the first panel of Fig. 3, again including all modes with frequencies below the maximum acoustic cutoff frequency. Again, we plot the log ratio of these against the corresponding integral estimates (this time from Eq. (17)) in Fig. 8. We see that for main-sequence stars, our estimator also adequately reproduces the fitted value of $\Delta\nu_l$. However, there is a considerable amount of scatter for stars that have evolved off the main sequence, as well as a clear systematic deviation for $l = 2$.

We attribute the above to difficulties in constructing a well-defined average $\Delta\nu$ for nonradial modes with evolved stars. For $l = 1$, avoided crossings emerge as the star evolves through the subgiant phase, and mixed-mode propagation (i.e. evanescent coupling to a g-mode cavity) becomes possible (Scuflaire 1974; Osaki 1975; Aizenman et al. 1977; Deheuvels & Michel 2011), with further mode splitting emerging when $\Delta\nu$ becomes sufficiently small. This g-mode coupling also changes the frequencies of observed $l = 2$ mixed modes relative to pure p-modes. Mixed modes are described by two quantum numbers n_p (the radial quantum number n of the p-mode being coupled) and n_g (Unno et al. 1989); in computing $\Delta\nu_l$, we have selected for each value of n_p the frequency of the corresponding mode with the lowest inertia. However, this does not necessarily correspond to the eigenfrequency of a pure p-mode with that value of n_p .

We illustrate this problem in Fig. 9, where we plot the ratio of the least-squares fitted values of $\Delta\nu_l$ to $\Delta\nu_0$ for $l = 1, 2$. It is clear that this ratio is relatively constant (although not necessarily unity) near the main sequence, but shows large variations — both systematic and in terms of scatter between timesteps — for evolved stars. Much of the scatter in Fig. 8 is a result of these rapid variations in $\Delta\nu_l$, rather than originating from our modified estimator. While our formulation cannot explain the remaining systematic differences for evolved stars (as in the bottom panel of Fig. 8, for $l = 2$), we nonetheless note that these have qualitatively the same morphology

as the relative differences between the sound-travel time and the fitted value of $\Delta\nu$. Again, this likely indicates limitations of our numerical formulation of the acoustic cutoff frequency; a careful accounting (as in Gough 1993) shows that it, too, depends on the degree l (in a somewhat complicated fashion), which is not included in our numerical integration.

4. CONCLUSIONS

We present a modified asymptotic expression, Eq. (16), as an estimator for $\Delta\nu$, the large frequency separation. We find that our estimator, evaluated at ν_{\max} , describes the large frequency separation (as obtained by fitting ν against n) more accurately than both the scaling relation and the classical asymptotic estimator, which is the sound travel time. While the latter can be modified to more closely match the fitted value by adjusting the integration domain somewhat arbitrarily, the turning points of our integral emerge naturally from the theoretical formulation, and do not suffer such ambiguity. This result appears to hold good with little variation with respect to choice of model atmosphere, and modifications to the model metallicity also do not substantially change the qualitative features of the residual deviation. The insensitivity of the residual differences to the choice of model atmosphere indicates that they originate from theoretical issues pertaining to the interior of the stellar models, rather than the surface, as is usually assumed (Hekker et al. 2013).

We also find that our integral expression becomes singular at some point during main-sequence turnoff; this failure mode is ultimately a consequence of the failure of the WKB regime under these conditions. We show that these singular points occur during a transition between two extreme regimes of asymptotic behavior, owing to structural evolution yielding a qualitative change in the inner turning point of the WKB integral. We argue that this provides theoretical justification for separately calibrated scaling relations for stars at different evolutionary stages.

Moreover, our naive application of the WKB approach appears insufficient to completely describe the behavior of $\Delta\nu$ as fitted from nonradial modes, particularly away from the main sequence. However, this may be improved with a more detailed numerical implementation. In any case, such a fit is observationally ill-defined away from the main sequence.

These limitations notwithstanding, we propose the use of this integral expression as an alternative to both the scaling relation and the sound-travel time for estimating $\Delta\nu$, although care should be taken to avoid the singular points where it fails. This expression is particularly well-suited to such a use when fitting stellar models to individual mode frequencies, in that the closeness of a model's $\Delta\nu$ to observed values can be used as a decision

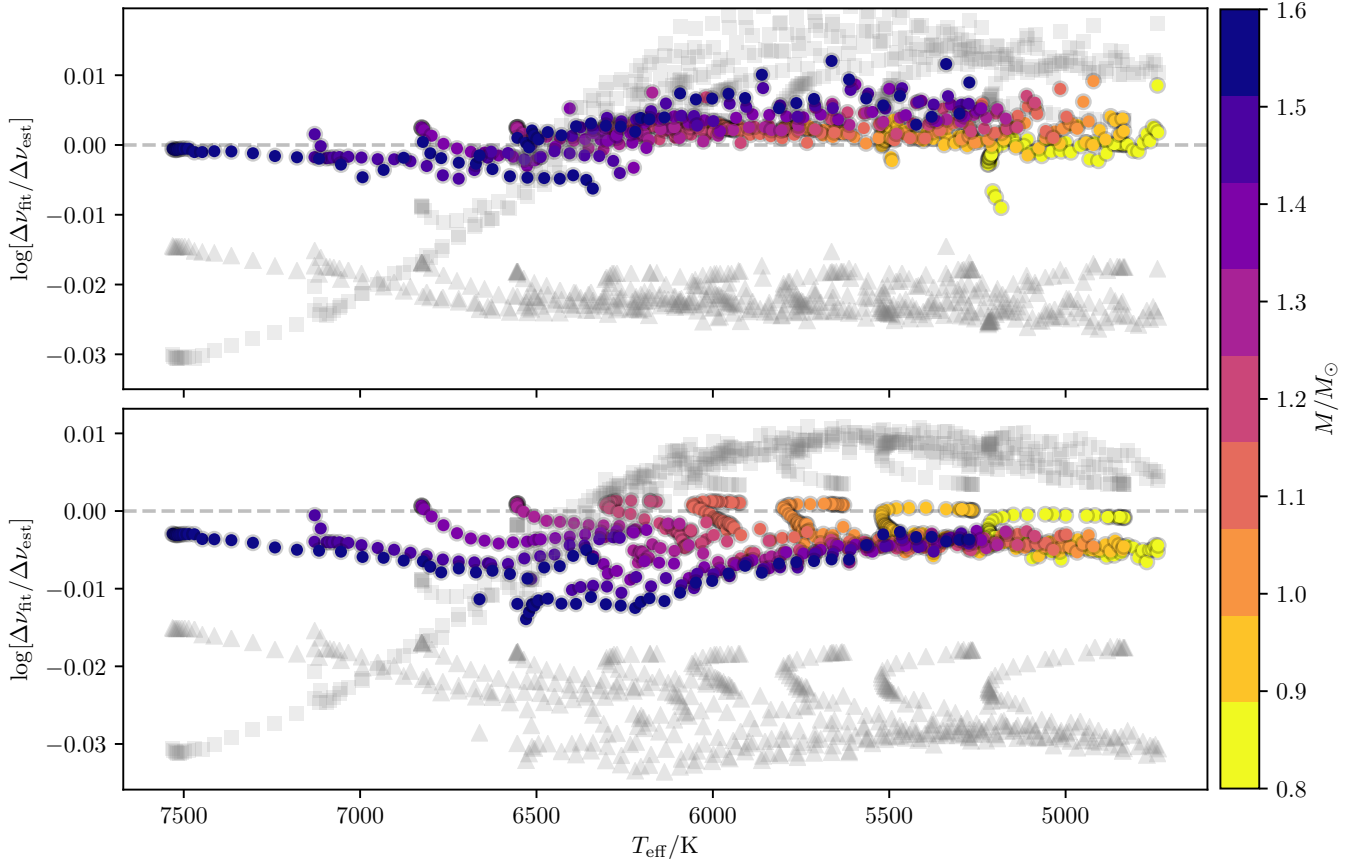


Figure 8. Log ratio of fitted $\Delta\nu$ versus various estimators, with the same coloring and markers as in Fig. 3. **Top:** Ratios for $\Delta\nu$ fitted from, and integral expressions with, $l = 1$. **Bottom:** The same with $l = 2$.

criterion for whether or not said model is sufficiently optimal as to warrant expending additional computational resources to calculate its individual mode frequencies. An accurate asymptotic estimation of $\Delta\nu$ will considerably reduce the size of this expensive search space.

The authors thank the referee, Dr. B. Mosser, for the very helpful comments and suggestions. This work was partially supported by NSF grant AST-1514676 and NASA grant NNX16AI09G to S.B.

Software: SciPy stack (Jones et al. 2001–), MESA (Paxton et al. 2015), GYRE (Townsend & Teitler 2013).

REFERENCES

- Aerts, C., Christensen-Dalsgaard, J., & Kurtz, D. W. 2010, *Asteroseismology* (Springer Netherlands)
- Aizenman, M., Smeyers, P., & Weigert, A. 1977, *A&A*, 58, 41
- Basu, S., Grundahl, F., Stello, D., et al. 2011, *ApJL*, 729, L10, doi: [10.1088/2041-8205/729/1/L10](https://doi.org/10.1088/2041-8205/729/1/L10)
- Belkacem, K., Goupil, M. J., Dupret, M. A., et al. 2011, *A&A*, 530, A142, doi: [10.1051/0004-6361/201116490](https://doi.org/10.1051/0004-6361/201116490)
- Belkacem, K., Samadi, R., Mosser, B., Goupil, M.-J., & Ludwig, H.-G. 2013, in *Astronomical Society of the Pacific Conference Series*, Vol. 479, *Progress in Physics of the Sun and Stars: A New Era in Helio- and Asteroseismology*, ed. H. Shibahashi & A. E. Lynas-Gray, 61
- Brown, T. M., Gilliland, R. L., Noyes, R. W., & Ramsey, L. W. 1991, *ApJ*, 368, 599, doi: [10.1086/169725](https://doi.org/10.1086/169725)
- Chaplin, W. J., Appourchaux, T., Elsworth, Y., et al. 2010, *ApJL*, 713, L169, doi: [10.1088/2041-8205/713/2/L169](https://doi.org/10.1088/2041-8205/713/2/L169)
- Chaplin, W. J., Basu, S., Huber, D., et al. 2014, *ApJS*, 210, 1, doi: [10.1088/0067-0049/210/1/1](https://doi.org/10.1088/0067-0049/210/1/1)
- Christensen-Dalsgaard, J. 1988, in *IAU Symposium*, Vol. 123, *Advances in Helio- and Asteroseismology*, ed. J. Christensen-Dalsgaard & S. Frandsen, 295
- Christensen-Dalsgaard, J., & Perez Hernandez, F. 1992, *MNRAS*, 257, 62, doi: [10.1093/mnras/257.1.62](https://doi.org/10.1093/mnras/257.1.62)
- Deheuvels, S., & Michel, E. 2011, *A&A*, 535, A91, doi: [10.1051/0004-6361/201117232](https://doi.org/10.1051/0004-6361/201117232)

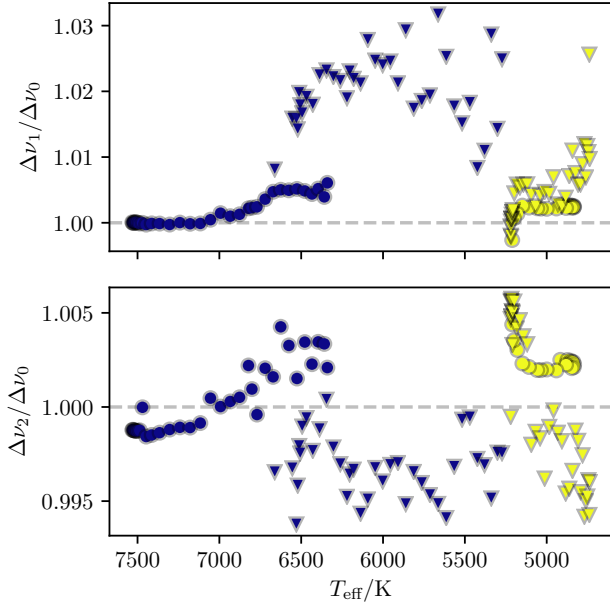


Figure 9. Ratios of $\Delta\nu_l$ to $\Delta\nu_0$ for $l = 1$ (top) and $l = 2$ (bottom), for evolutionary tracks of stellar masses 0.8 and $1.6 M_\odot$, with colors corresponding to the earlier figures Fig. 3. Main-sequence models are denoted with circles, while subgiants (with core hydrogen mass fractions $X < 10^{-4}$) are shown with inverted triangles.

- Deubner, F.-L., & Gough, D. 1984, ARA&A, 22, 593, doi: [10.1146/annurev.aa.22.090184.003113](https://doi.org/10.1146/annurev.aa.22.090184.003113)
- Gough, D. O. 1993, in *Astrophysical Fluid Dynamics - Les Houches 1987*, ed. J.-P. Zahn & J. Zinn-Justin, 399–560
- Gough, D. O. 2007, *Astronomische Nachrichten*, 328, 273, doi: [10.1002/asna.200610730](https://doi.org/10.1002/asna.200610730)
- Grevesse, N., & Sauval, A. J. 1998, *SSRv*, 85, 161, doi: [10.1023/A:1005161325181](https://doi.org/10.1023/A:1005161325181)
- Guggenberger, E., Hekker, S., Angelou, G. C., Basu, S., & Bellinger, E. P. 2017, *MNRAS*, 470, 2069, doi: [10.1093/mnras/stx1253](https://doi.org/10.1093/mnras/stx1253)
- Guggenberger, E., Hekker, S., Basu, S., & Bellinger, E. 2016, *MNRAS*, 460, 4277, doi: [10.1093/mnras/stw1326](https://doi.org/10.1093/mnras/stw1326)
- Hekker, S., Elsworth, Y., Basu, S., et al. 2013, *MNRAS*, 434, 1668, doi: [10.1093/mnras/stt1238](https://doi.org/10.1093/mnras/stt1238)
- Jones, E., Oliphant, T., Peterson, P., et al. 2001–, SciPy: Open source scientific tools for Python. <http://www.scipy.org/>
- Kallinger, T., Beck, P. G., Stello, D., & Garcia, R. A. 2018, *A&A*, 616, A104, doi: [10.1051/0004-6361/201832831](https://doi.org/10.1051/0004-6361/201832831)
- Kjeldsen, H., & Bedding, T. R. 1995, *A&A*, 293, 87
- Miglio, A., Brogaard, K., Stello, D., et al. 2012, *MNRAS*, 419, 2077, doi: [10.1111/j.1365-2966.2011.19859.x](https://doi.org/10.1111/j.1365-2966.2011.19859.x)
- Osaki, J. 1975, *PASJ*, 27, 237
- Paxton, B., Marchant, P., Schwab, J., et al. 2015, *ApJS*, 220, 15, doi: [10.1088/0067-0049/220/1/15](https://doi.org/10.1088/0067-0049/220/1/15)
- Pinsonneault, M. H., Elsworth, Y., Epstein, C., et al. 2014, *ApJS*, 215, 19, doi: [10.1088/0067-0049/215/2/19](https://doi.org/10.1088/0067-0049/215/2/19)
- Roxburgh, I. W., & Vorontsov, S. V. 1994, *MNRAS*, 268, 143, doi: [10.1093/mnras/268.1.143](https://doi.org/10.1093/mnras/268.1.143)
- Scuflaire, R. 1974, *A&A*, 36, 107
- Serenelli, A., Johnson, J., Huber, D., et al. 2017, *ApJS*, 233, 23, doi: [10.3847/1538-4365/aa97df](https://doi.org/10.3847/1538-4365/aa97df)
- Sharma, S., Stello, D., Bland-Hawthorn, J., Huber, D., & Bedding, T. R. 2016, *ApJ*, 822, 15, doi: [10.3847/0004-637X/822/1/15](https://doi.org/10.3847/0004-637X/822/1/15)
- Tassoul, M. 1994, *ApJ*, 421, 390, doi: [10.1086/173657](https://doi.org/10.1086/173657)
- Townsend, R. H. D., & Teitler, S. A. 2013, *MNRAS*, 435, 3406, doi: [10.1093/mnras/stt1533](https://doi.org/10.1093/mnras/stt1533)
- Ulrich, R. K. 1986, *ApJL*, 306, L37, doi: [10.1086/184700](https://doi.org/10.1086/184700)
- Unno, W., Osaki, Y., Ando, H., Saio, H., & Shibahashi, H. 1989, *Nonradial oscillations of stars*
- White, T. R., Bedding, T. R., Stello, D., et al. 2011, *ApJ*, 743, 161, doi: [10.1088/0004-637X/743/2/161](https://doi.org/10.1088/0004-637X/743/2/161)